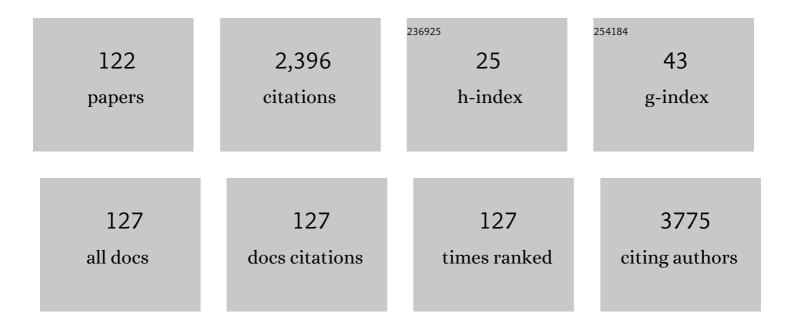


## List of Publications by Year in descending order

Source: https://exaly.com/author-pdf/3951186/publications.pdf Version: 2024-02-01



Химс Мл

#	Article	IF	CITATIONS
1	Pressure-induced semiconducting to metallic transition in multilayered molybdenum disulphide. Nature Communications, 2014, 5, 3731.	12.8	495
2	High-pressure behavior of iron carbide (Fe <sub>7</sub> C <sub>3</sub> ) at inner core conditions. Journal of Geophysical Research, 2011, 116, .	3.3	75
3	Selfâ€Assembled Alluaudite Na <sub>2</sub> Fe <sub>3â``<i>x</i></sub> Mn <sub><i>x</i></sub> (PO <sub>4</sub> ) <sub>3</sub> Micro/Nanocompounds for Sodiumâ€ion Battery Electrodes: A New Insight into Their Electronic and Geometric Structure. Chemistry - A European Iournal. 2015. 21. 851-860.	3.3	63
4	Pressure-induced phase transformation of CsPbI <sub>3</sub> by X-ray diffraction and Raman spectroscopy. Phase Transitions, 2018, 91, 38-47.	1.3	61
5	K-ĥ crossover transition in the conduction band of monolayer MoS <sub>2</sub> under hydrostatic pressure. Science Advances, 2017, 3, e1700162.	10.3	60
6	Micro-Raman study of perovskites in the CaTiO3–SrTiO3system. Dalton Transactions RSC, 2002, , 3751-3755.	2.3	52
7	Isotropic Negative Area Compressibility over Large Pressure Range in Potassium Beryllium Fluoroborate and its Potential Applications in Deep Ultraviolet Region. Advanced Materials, 2015, 27, 4851-4857.	21.0	52
8	First-principles study of structural stabilities, and electronic and optical properties ofCaF2under high pressure. Physical Review B, 2006, 73, .	3.2	48
9	Jahn–Teller Effect on Framework Flexibility of Hybrid Organic–Inorganic Perovskites. Journal of Physical Chemistry Letters, 2018, 9, 751-755.	4.6	47
10	Dual‣timuliâ€Responsive Photoluminescence of Enantiomeric Twoâ€Dimensional Lead Halide Perovskites. Advanced Optical Materials, 2021, 9, 2100003.	7.3	38
11	Structural stability of a golden semiconducting orthorhombic polymorph of Ti <sub>2</sub> O <sub>3</sub> under high pressures and high temperatures. Journal of Physics Condensed Matter, 2010, 22, 375402.	1.8	37
12	Distance makes a difference in crystalline photoluminescence. Nature Communications, 2020, 11, 5572.	12.8	37
13	High-pressure behavior of Fe3P and the role of phosphorus in planetary cores. Earth and Planetary Science Letters, 2014, 390, 296-303.	4.4	34
14	High-pressure phase transitions and compressibilities of aragonite-structure carbonates: SrCO3 and BaCO3. Physics and Chemistry of Minerals, 2015, 42, 517-527.	0.8	33
15	First-principles study of the pressure-induced phase transition in CaTiO3. Solid State Communications, 2005, 136, 416-420.	1.9	32
16	Pressure-induced phase transformation in controlled shape ZnO nanorods. Solid State Communications, 2005, 135, 780-784.	1.9	32
17	High pressure structural study of β-Ti3O5: X-ray diffraction and Raman spectroscopy. Journal of Solid State Chemistry, 2012, 192, 356-359.	2.9	31
18	Preparation and thermal characterization of sodium acetate trihydrate/expanded graphite composite phase change material. Journal of Thermal Analysis and Calorimetry, 2016, 125, 831-838.	3.6	31

#	Article	IF	CITATIONS
19	Structural stability of TiO2at high pressure in density-functional theory based calculations. Journal of Physics Condensed Matter, 2010, 22, 295501.	1.8	30
20	High-T <sub>c</sub> ferromagnetism in a Co-doped ZnO system dominated by the formation of a zinc-blende type Co-rich ZnCoO phase. Chemical Communications, 2012, 48, 91-93.	4.1	30
21	Spin transition of ferric iron in the NAL phase: Implications for the seismic heterogeneities of subducted slabs in the lower mantle. Earth and Planetary Science Letters, 2016, 434, 91-100.	4.4	30
22	Structural characterization of the FeTiO3–MnTiO3 solid solution. Journal of Solid State Chemistry, 2010, 183, 2483-2489.	2.9	29
23	Negative linear compressibility in a crystal of α-BiB3O6. Scientific Reports, 2015, 5, 13432.	3.3	28
24	Highâ€pressure Raman spectra of tuite, γ a <sub>3</sub> (PO <sub>4</sub> ) <sub>2</sub> . Journal of Raman Spectroscopy, 2010, 41, 1011-1013.	2.5	26
25	Investigation into high-pressure behavior of MnTiO3: X-ray diffraction and Raman spectroscopy with diamond anvil cells. Geoscience Frontiers, 2011, 2, 107-114.	8.4	26
26	High pressure behaviour and elastic properties of a dense inorganic–organic framework. Dalton Transactions, 2016, 45, 4303-4308.	3.3	26
27	Equation of state and hyperfine parameters of high-spin bridgmanite in the Earth's lower mantle by synchrotron X-ray diffraction and Mössbauer spectroscopy. American Mineralogist, 2017, 102, 357-368.	1.9	26
28	In situ high-pressure study of FeP: Implications for planetary cores. Physics of the Earth and Planetary Interiors, 2011, 184, 154-159.	1.9	24
29	High-pressure behavior of structural, optical, and electronic transport properties of the golden Th2S3-type Ti2O3. Physical Review B, 2013, 88, .	3.2	24
30	Confirming a pyrolitic lower mantle using selfâ€consistent pressure scales and new constraints on CaSiO <sub>3</sub> perovskite. Journal of Geophysical Research: Solid Earth, 2016, 121, 4876-4894.	3.4	24
31	Compressibility of Cs 2 SnBr 6 by X-ray diffraction and Raman spectroscopy. Solid State Communications, 2018, 275, 68-72.	1.9	24
32	Highly Active Surface Structure in Nanosized Spinel Cobalt-Based Oxides for Electrocatalytic Water Splitting. Journal of Physical Chemistry C, 2018, 122, 14447-14458.	3.1	24
33	High-temperature Raman and FTIR study of aragonite-group carbonates. Physics and Chemistry of Minerals, 2019, 46, 51-62.	0.8	24
34	Pressure-temperature phase diagram of Ti2O3and physical properties in the golden Th2S3-type phase. Physical Review B, 2012, 86, .	3.2	22
35	Compressibility of a natural smithsonite ZnCO <sub>3</sub> up to 50ÂGPa. High Pressure Research, 2014, 34, 89-99.	1.2	22
36	Zero Linear Compressibility in Nondense Borates with a "Luâ€Ban Stoolâ€â€Łike Structure. Advanced Materials, 2018, 30, e1801313.	21.0	22

#	Article	IF	CITATIONS
37	Structural, Optical, and Thermal Properties of Cs <sub>2</sub> SnI <sub>6</sub> <sub>–</sub> <sub><i>x</i>/i&gt;</sub> Br <i><sub>x</sub></i> Mixed Perovskite Solid Solutions. European Journal of Inorganic Chemistry, 2019, 2019, 2524-2529.	2.0	21
38	Suppression of Bragg reflection glitches of a single-crystal diamond anvil cell by a polycapillary half-lens in high-pressure XAFS spectroscopy. Journal of Synchrotron Radiation, 2013, 20, 243-248.	2.4	20
39	Seismic anisotropy of the D″ layer induced by (001) deformation of post-perovskite. Nature Communications, 2017, 8, 14669.	12.8	20
40	Tuning Pressure-Induced Phase Transitions, Amorphization, and Excitonic Emissions of 2D Hybrid Perovskites via Varying Organic Amine Cations. Journal of Physical Chemistry C, 2019, 123, 22491-22498.	3.1	19
41	Raman spectra and X-ray diffraction of tuite at various temperatures. Physics and Chemistry of Minerals, 2011, 38, 639-646.	0.8	17
42	New high-pressure polymorph of In2S3 with defect Th3P4-type structure. Journal of Solid State Chemistry, 2014, 210, 155-159.	2.9	17
43	Compressibility of carbonophosphate bradleyite Na3Mg(CO3)(PO4) by X-ray diffraction and Raman spectroscopy. Physics and Chemistry of Minerals, 2015, 42, 191-201.	0.8	16
44	High-pressure behavior of natural single-crystal epidote and clinozoisite up to 40 GPa. Physics and Chemistry of Minerals, 2016, 43, 649-659.	0.8	16
45	Phase stabilities and spin transitions of Fe <sub>3</sub> (S <sub>1â^'x</sub> P <sub>x</sub> ) at high pressure and its implications in meteorites. American Mineralogist, 2016, 101, 205-210.	1.9	16
46	Generalized gradient approximation calculations of the pressure-induced phase transition of YAlO3perovskite. Journal of Physics Condensed Matter, 2006, 18, 3907-3916.	1.8	15
47	High-pressure powder x-ray diffraction experiments and <i>ab initio</i> calculation of Ti3AlC2. Journal of Applied Physics, 2009, 106, .	2.5	15
48	X-ray diffraction study of -Ca3(PO4)2 at high pressure. Solid State Communications, 2010, 150, 443-445.	1.9	15
49	Structural and elastic properties of CaGeO3 perovskite at high pressures. Physics of the Earth and Planetary Interiors, 2011, 189, 151-156.	1.9	15
50	Pressure-dependent Raman spectra of β-Ca3(PO4)2 whitlockite. Physics and Chemistry of Minerals, 2015, 42, 303-308.	0.8	15
51	A re-investigation on pressure-induced phase transition of Mg2Si. Solid State Communications, 2012, 152, 2160-2164.	1.9	14
52	Probing nonequivalent sites in iron phosphide Fe2P and its mechanism of phase transition. European Physical Journal B, 2013, 86, 1.	1.5	13
53	Raman spectra of sillimanite, andalusite, and kyanite at various temperatures. Physics and Chemistry of Minerals, 2020, 47, 1.	0.8	13
54	First-principles calculations of the structural stability of Fe <sub>2</sub> P. Journal of Physics: Conference Series, 2010, 215, 012110.	0.4	12

#	Article	IF	CITATIONS
55	Twoâ€stage spin transition of iron in FeAlâ€bearing phase D at lower mantle. Journal of Geophysical Research: Solid Earth, 2016, 121, 6411-6420.	3.4	12
56	Thermal Equation of State of Natural Tiâ€Bearing Clinohumite. Journal of Geophysical Research: Solid Earth, 2017, 122, 8943-8951.	3.4	12
57	Pressure-induced drastic collapse of a high oxygen coordination shell in quartz-like <i>î±</i> -GeO <sub>2</sub> . New Journal of Physics, 2014, 16, 023022.	2.9	11
58	Compressibilities of MnFe2O4 polymorphs. Physics and Chemistry of Minerals, 2015, 42, 569-577.	0.8	11
59	The crystal chemistry and the compressibility of silicate-carbonate minerals: Spurrite, galuskinite and tilleyite. Geoscience Frontiers, 2015, 6, 771-777.	8.4	11
60	Petrofabrics and Seismic Properties of Himalayan Amphibolites: Implications for a Thick Anisotropic Deep Crust Beneath Southern Tibet. Journal of Geophysical Research: Solid Earth, 2020, 125, e2019JB018700.	3.4	11
61	Pressure-Induced Phase Transition of V <sub>2</sub> O <sub>3</sub> . Chinese Physics Letters, 2012, 29, 106101.	3.3	10
62	Compressibility and phase transition of intermetallic compound Fe2Ti. Journal of Alloys and Compounds, 2013, 558, 160-163.	5.5	10
63	Structural phase transition and microwave dielectric properties of Ca1â^'x Sr x TiO3 (xÂ=Â0.1–0.9) ceramics. Journal of Materials Science: Materials in Electronics, 2015, 26, 1507-1511.	2.2	10
64	Pressure-induced structural and spin transitions of Fe3S4. Scientific Reports, 2017, 7, 46334.	3.3	10
65	Ultrahighâ€Pressure Phase Transitions in FeS <sub>2</sub> and FeO <sub>2</sub> : Implications for Superâ€Earths' Deep Interior. Journal of Geophysical Research: Solid Earth, 2018, 123, 277-284.	3.4	10
66	Structural, magnetic and electronic properties of CrO <sub>2</sub> at multimegabar pressures. RSC Advances, 2018, 8, 24561-24570.	3.6	10
67	Pressure-induced phase transition of La <sub>2</sub> Zr <sub>2</sub> O <sub>7</sub> and La <sub>0.5</sub> Gd <sub>1.5</sub> Zr <sub>2</sub> O <sub>7</sub> pyrochlore. RSC Advances, 2019, 9, 18954-18962.	3.6	10
68	Raman spectra and X-ray diffraction of merrillite at various temperatures. Vibrational Spectroscopy, 2020, 106, 103005.	2.2	10
69	Pressure-induced phase transition of Fe2TiO4: X-ray diffraction and Mössbauer spectroscopy. Journal of Solid State Chemistry, 2012, 185, 72-75.	2.9	9
70	Equation of state of a synthetic ulvöspinel, (Fe1.94Ti0.03)Ti1.00O4.00, at ambient temperature. Physics and Chemistry of Minerals, 2015, 42, 171-177.	0.8	9
71	High-Pressure and High-Temperature <i>in situ</i> X-Ray Diffraction Study of FeP <sub>2</sub> up to 70 GPa. Chinese Physics Letters, 2012, 29, 026102.	3.3	8
72	Hydrogen-Bond Symmetrization of <i><math>\hat{I}</math> </i> -AlOOH. Chinese Physics Letters, 2017, 34, 108301.	3.3	8

#	Article	IF	CITATIONS
73	Stability and anisotropy of (FexNi1â^'x)2O under high pressure and implications in Earth's and super-Earths' core. Scientific Reports, 2018, 8, 236.	3.3	8
74	Experimental and theoretical investigation on the compression mechanism of FeF <sub>3</sub> up to 62.0â€GPa. Acta Crystallographica Section B: Structural Science, Crystal Engineering and Materials, 2014, 70, 801-808.	1.1	7
75	Elasticity of singleâ€crystal NAL phase at high pressure: A potential source of the seismic anisotropy in the lower mantle. Journal of Geophysical Research: Solid Earth, 2016, 121, 5696-5707.	3.4	7
76	High mechanical strength in Zn <sub>4</sub> B <sub>6</sub> O <sub>13</sub> with an unique sodalite-cage structure. RSC Advances, 2017, 7, 2038-2043.	3.6	7
77	Spin transition of ferric iron in the calciumâ€ferrite type aluminous phase. Journal of Geophysical Research: Solid Earth, 2017, 122, 5935-5944.	3.4	7
78	Ultradeep diamonds originate from deep subducted sedimentary carbonates. Science China Earth Sciences, 2017, 60, 207-217.	5.2	7
79	Pressure-induced reversible phase transition on Mo2Ga2C. Journal of Applied Physics, 2018, 124, .	2.5	7
80	Elasticity and Anisotropy of the Pyrite-Type FeO2H-FeO2 System in Earth's Lowermost Mantle. Journal of Earth Science (Wuhan, China), 2019, 30, 1293-1301.	3.2	7
81	Structural Modifications of Single-Crystal Aragonite CaCO3 Beginning at ~15 GPa: In Situ Vibrational Spectroscopy and X-Ray Diffraction Evidence. Minerals (Basel, Switzerland), 2020, 10, 924.	2.0	7
82	Elasticity and anisotropy of iron-nickel phosphides at high pressures. Geophysical Research Letters, 2011, 38, n/a-n/a.	4.0	6
83	First-principles investigation on high-pressure structural evolution of MnTiO3. Solid State Communications, 2012, 152, 984-988.	1.9	6
84	In situ XAFS Investigation on Zincblende ZnS up to 31.7 GPa. Chinese Physics Letters, 2013, 30, 046101.	3.3	6
85	Experimental and theoretical identification of a high-pressure polymorph of Ga2S3 with α-Bi2Te3-type structure. Journal of Applied Physics, 2014, 116, 193507.	2.5	6
86	Experimental and theoretical investigations on high-pressure phase transition of Sr2Fe2O5. Physics and Chemistry of Minerals, 2014, 41, 449-459.	0.8	6
87	Phase relations of the nepheline-kalsilite system: X-ray diffraction and Mössbauer spectroscopy. Journal of Alloys and Compounds, 2017, 712, 613-617.	5.5	6
88	Pressure-Induced Phase Transition in Mn(Ta,Nb) <sub>2</sub> O <sub>6</sub> : An Experimental Investigation and First-Principle Study. Inorganic Chemistry, 2020, 59, 18122-18130.	4.0	6
89	A nine-fold coordinated vanadium by oxygen in V2O3 from first-principles calculations. European Physical Journal B, 2012, 85, 1.	1.5	5
90	Pressure-induced phase transitions of multiferroic BiFeO <sub>3</sub> . Chinese Physics C, 2013, 37, 128001.	3.7	5

#	Article	IF	CITATIONS
91	High-pressure, high-temperature synthesis and properties of the monoclinic phase of Y2O3. Chemical Research in Chinese Universities, 2016, 32, 545-548.	2.6	5
92	High pressure experimental studies on Na3Fe(PO4)(CO3) and Na3Mn(PO4)(CO3): Extensive pressure behaviors of carbonophosphates family. Journal of Physics and Chemistry of Solids, 2018, 115, 248-253.	4.0	5
93	Compressibility of natural schreibersite up to 50 GPa. Physics and Chemistry of Minerals, 2019, 46, 91-99.	0.8	5
94	Temperature-induced phase transition of Ca2AlSiO5.5: Raman spectroscopic study. Vibrational Spectroscopy, 2019, 103, 102935.	2.2	5
95	Thermal Behavior of Pyromorphite (Pb10(PO4)6Cl2): In Situ High Temperature Powder X-ray Diffraction Study. Crystals, 2020, 10, 1070.	2.2	5
96	Fate of Carbonates in the Earth's Mantle (10-136 GPa). Frontiers in Earth Science, 2022, 10, .	1.8	5
97	Quasi-hydrostatic Limit of LiF as a Pressure Transmitting Medium and Its Equation of States. Chinese Physics Letters, 2014, 31, 056201.	3.3	4
98	Phase, microstructure and microwave dielectric properties of A-site deficient (La, Nd)2/3TiO3 perovskite ceramics. Materials Science-Poland, 2015, 33, 126-130.	1.0	4
99	High pressure structural investigation on alluaudites Na 2 Fe 3 (PO 4 ) 3 -Na 2 FeMn 2 (PO 4 ) 3 system. Journal of Solid State Chemistry, 2017, 247, 156-160.	2.9	4
100	Thermal stability and compressibility of bastnaesite. Physics and Chemistry of Minerals, 2020, 47, 1.	0.8	4
101	Phase transition of Mg3(PO4)2 polymorphs at high-temperature: In-situ synchrotron X-ray diffraction and Raman spectroscopic study. Spectrochimica Acta - Part A: Molecular and Biomolecular Spectroscopy, 2022, 269, 120762.	3.9	4
102	High pressure X-ray diffraction study of SrMnO 3 perovskite. Chinese Physics C, 2011, 35, 514-518.	3.7	3
103	Pressure-induced phase transition and dissociation of PbMoO4. Physica Status Solidi (B): Basic Research, 2015, 252, 2215-2221.	1.5	3
104	Compressional behavior of natural eclogitic zoisite by synchrotron X-ray single-crystal diffraction to 34 GPa. Physics and Chemistry of Minerals, 2019, 46, 333-341.	0.8	3
105	Phase transition of sanidine (KAlSi3O8) and its effect on electrical conductivity at pressures up to 11ÂGPa. Physics and Chemistry of Minerals, 2020, 47, 1.	0.8	3
106	Highâ€Pressure Phase Stability and Thermoelastic Properties of Iron Carbonitrides and Nitrogen in the Deep Earth. Journal of Geophysical Research: Solid Earth, 2021, 126, e2021JB021934.	3.4	3
107	Partial dehydration of brucite and its implications for water distribution in the subducting oceanic slab. Geoscience Frontiers, 2022, 13, 101342.	8.4	3
108	Raman spectroscopic and X-ray diffraction study of α- and β-Mg2P2O7 at various temperatures. Spectrochimica Acta - Part A: Molecular and Biomolecular Spectroscopy, 2022, 273, 121076.	3.9	3

#	Article	IF	CITATIONS
109	Pressure- and temperature-dependent Raman spectra of Ca2Fe2O5 oxygen defect perovskite. Spectrochimica Acta - Part A: Molecular and Biomolecular Spectroscopy, 2022, 279, 121436.	3.9	3
110	In situ high-pressure X-ray diffraction experiments and ab initio calculations of Co 2 P. Chinese Physics B, 2011, 20, 066101.	1.4	2
111	Compressibility of a natural P4/nnc vesuvianite. European Journal of Mineralogy, 2013, 25, 631-637.	1.3	2
112	X-ray diffraction studies of Sr3Cr2O8 and Ba3Cr2O8 at high pressures. Solid State Communications, 2014, 200, 5-8.	1.9	2
113	High-pressure phase transitions of natural chromitite from Tibetan ophiolites. Lithos, 2018, 320-321, 20-27.	1.4	2
114	X-ray diffraction and Raman spectra of merrillite at high pressures. High Pressure Research, 2020, 40, 411-422.	1.2	2
115	Thermal equation of state of phase egg (AlSiO3OH): implications for hydrous phases in the deep earth. Contributions To Mineralogy and Petrology, 2021, 176, 1.	3.1	2
116	Processing and characterization of A-site deficient [(Ca, Sr) x (La, Nd)2/3â^'2x/3]TiO3 dielectric ceramics. Journal of Materials Science: Materials in Electronics, 2014, 25, 5282-5287.	2.2	1
117	Magnetism-Vanishing Stabilizes the Pyrite-Type 3d Transition Metal Peroxides at High Pressures. Journal of Physical Chemistry C, 2020, 124, 10085-10093.	3.1	1
118	Thermal equation of state of F-bearing superhydrous phase B (Mg10Si3O14(OH,F)4): Implications for the transportation of fluorine and water into the lower mantle. Physics of the Earth and Planetary Interiors, 2022, 323, 106824.	1.9	1
119	Structural characteristics and elasticities of coesite and coesite-II at high pressure. New Journal of Physics, 2020, 22, 093044.	2.9	1
120	Phase transition of intermetallic TbPt at high temperature and high pressure. Journal of Physics Condensed Matter, 2018, 30, 144001.	1.8	0
121	Pressure-induced dehydration of dioptase: A single-crystal X-ray diffraction and Raman spectroscopy study. Comptes Rendus - Geoscience, 2019, 351, 121-128.	1.2	0
122	CO 2 Induced a Small Water Solubility in Orthopyroxene and Its Implications for Water Storage in the Upper Mantle. Journal of Geophysical Research: Solid Earth, 2020, 125, e2019JB018745.	3.4	0